Nuclear Instruments and Methods in Physics Research A 683 (2012) 53–62

Contents lists available at SciVerse ScienceDirect

Nuclear Instruments and Methods in Physics Research A

journal homepage: www.elsevier.com/locate/nima

Impact of drift time variation on the Compton image from large-volume CdZnTe crystals

Jae Cheon Kim *, William R. Kaye, Weiyi Wang, Feng Zhang, Zhong He

Department of Nuclear Engineering and Radiological Sciences, University of Michigan, Ann Arbor, MI 48109, USA

ARTICLE INFO

Article history:
Received 30 September 2011
Received in revised form
18 April 2012
Accepted 21 April 2012
Available online 8 May 2012

Keywords:
Semiconductor detector
CdZnTe
Electron drift velocity
Drift time variation
Three-dimensional (3D) position-sensitive
Cathode waveform
Multiple-pixel events
Compton imaging

ABSTRACT

In pixelated CdZnTe detectors, multiple interaction gamma-ray events are critical because they permit Compton imaging. However, in large-volume CdZnTe crystals, the depth of multiple interaction events is often poorly reconstructed due to significant nonuniformity of electron drift velocity while the depth of single interaction events can be accurately reconstructed using signal ratios. The nonuniformity of the drift velocity is likely due to nonuniformity in the electric field within the detector. This causes variation in the drift time even amongst events that occur at the same depth of interaction in the same pixel. The degradation in the depth reconstruction results in poorer imaging performance. The electron drift velocity at each depth is measured using ^{241}Am alpha particles incident on the entire cathode surface of each detector. Cathode waveforms are recorded for events collected by each element in the 11×11 array of anode pixels. To illustrate the impact of electron drift time variation, two CdZnTe crystals fabricated by Redlen Technologies with similar spectral performance, but significantly different Compton imaging performance are selected. The detector with poorer imaging performance demonstrated significant nonuniformity of the electron drift velocity. This work clearly shows that even CdZnTe crystals with 1% FWHM energy resolution at 662 keV can have a nonuniform electron drift velocity, on the sub-pixel scale, which seriously degrades the Compton imaging performance of pixelated detectors.

1. Introduction

The Polaris project at the University of Michigan uses pixelated 3D position-sensitive CdZnTe detectors to perform high resolution gamma-ray spectroscopy and 4π Compton imaging [1,2]. In order to achieve these capabilities, a three-dimensional (3D) position-sensing technique and large-volume single crystal CdZnTe detectors with extended thickness are required [3]. However, high concentrations of extended defects such as twins, subgrain boundaries, Te inclusions, and dislocations have been observed in large-volume CdZnTe crystals [4,5]. In addition, it is reported that nonuniform internal electric field due to local perturbations by the presence of extended defects and residual strains existing inside the crystals can be a significant factor degrading performance of CdZnTe detectors [6,7].

Recently, more than 100 CdZnTe detectors from Redlen Technologies have been evaluated at the University of Michigan. The imaging performance between detectors is found to vary significantly, even amongst detectors with good spectroscopic performance. Thus, there is a mechanism that significantly impacts the imaging performance of some detectors without significantly degrading the spectroscopic performance. This work will show that this is due, at least in part, to invalid reconstruction of the depth of interaction due to variations in electron drift time. Other work has shown that drift time variations can degrade the energy resolution [8], but this work focuses on two detectors that have similar energy resolution and significantly different angular resolution in the Compton image.

In pixelated CdZnTe detectors, single- and multiple-pixel events are determined by the number of pixels triggered by each incident gamma-ray interaction. Fig. 1 shows the anode array pattern with a noncollecting steering grid applied to the CdZnTe crystals used at the University of Michigan. In order to understand the degradation in the Compton image quality of certain detectors it is important to consider the nature of event reconstruction in the system. Compton imaging information is only available for gamma rays that interact at least twice in the detector. This means that the events useful for imaging involve information from multiple pixels, and are thus referred to as multiple-pixel events.

Multiple-pixel events occur by either multiple gamma-ray interactions or charge-sharing of a single electron cloud between adjacent pixels. The energy and position reconstruction of multiple-pixel events is an important factor that limits the spectral

* Corresponding author.
E-mail address: jaecheon@umich.edu (J.C. Kim).

0168-9002/$ - see front matter © 2012 Elsevier B.V. All rights reserved.
http://dx.doi.org/10.1016/j.nima.2012.04.057

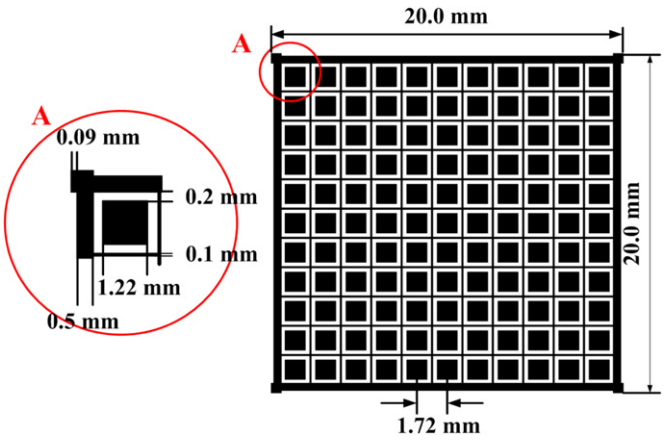

Fig. 1. Anode array pattern with a noncollecting steering grid applied to the CdZnTe crystals used at the University of Michigan, which have dimensions of 20 mm × 20 mm × 15 mm and include an 11 × 11 square pixel array fabricated on the anode surface with a pixel pitch of 1.72 mm.

performance and imaging capability of pixelated CdZnTe detectors [9]. Multiple-pixel events account for more than ~60% of the total photopeak counts at 662 keV in the detector geometry described in Fig. 1. The initial location of each charge cloud collected by a pixel is determined from the 2D coordinates of each collecting pixel and a measurement of the depth of interaction. The ratio of the cathode to the anode signal (C/A ratio) can be used to reconstruct the depth of interaction in the case of single-pixel events [10]. However, for multiple-pixel events, the electron drift times of each triggered pixel must be measured to determine the depth of interaction. The C/A ratio is directly proportional to depth and is mostly independent of the electron transport properties of the material, assuming that most electrons are collected within the shaping time of the cathode signal. However, the drift time measurement is influenced directly by the electron transport properties.

The total electron drift time, t_e, is the integral of the drift velocity along the electron drift trajectory, such that

$$t_e = \int_{z_i}^{T} \frac{1}{v_e(z)}\, dz \tag{1}$$

$$t_e = \int_{z_i}^{T} \frac{1}{\mu_e(z)E(z)}\, dz \tag{2}$$

$$t_e = \frac{1}{\mu_e}\int_{z_i}^{T} \frac{1}{E(z)}\, dz \tag{3}$$

where z_i is the initial depth of interaction measured from the cathode surface, T is the detector thickness, $v_e(z)$ is the electron drift velocity at depth z, $\mu_e(z)$ is the electron mobility, and $E(z)$ is the electric field at each depth. Eq. (2) is correct if the majority of electrons drift directly to the anode without undergoing trapping and detrapping. Eq. (3) can be used to describe the drift time given the additional assumption that mobility is constant throughout the detector volume. In this case, the drift velocity distribution at each depth is identical to the electric field distribution multiplied by a constant scaling factor. Eqs. (1)–(3) assume that the electrons drift directly from the cathode to the nearest anode pixel without lateral movement within the device. The lateral movement of electrons, which has already been measured directly in CdZnTe [7], will increase the overall drift time from cathode to anode and should be considered as a possible cause of drift time variations.

It is important to consider the relationship between variations in the drift velocity of electrons and the degradation of the depth reconstruction for multiple-pixel events. If the drift velocity changes as a function of depth, it is still possible to correctly reconstruct the depth of interaction if the drift time does not vary within a voxel, defined by the spatial resolution of the device. If the measured drift time does vary significantly within a voxel, then it is impossible to calibrate the relationship between drift time and position, which degrades the depth of interaction reconstruction from the drift time.

In this work, the VAS_UM/TAT4 ASIC [1] designed by Gamma-Medica Ideas is used to determine the interaction position. This readout ASIC limits the spatial resolution to the pixel pitch. Sub-pixel position resolution can be achieved by comparing the amplitude of transient signals in the noncollecting pixels [11], although this requires a system capable of extracting the pre-amplifier signal from each pixel.

It is critical to develop a technique that can identify detectors incapable of forming good Compton images. In principle, if the electron drift velocity is not uniform within the area of one pixel, then the recorded drift times from a single depth of interaction bin in a single pixel will vary significantly. It is possible to observe this behavior using gamma rays and measuring the drift time variance of each voxel within the detector. The goal of this work is to validate that the drift time variance calculated from gamma-ray data is due to nonuniform electron drift velocity and is one of the factors responsible for image quality degradation. Once this technique has been validated it can be applied to a data bank at the University of Michigan with gamma-ray test results for more than 150 large volume CdZnTe detectors from Redlen Technologies.

An alpha source is used to prove the correlation between the drift time variance measured with an ASIC and nonuniformity of the electron drift velocity. A large number of alpha waveforms are collected for each pixel and their drift profile is studied to determine the variation in velocity as a function of depth. Finally, a Compton image is generated for each detector in order to prove how this drift velocity variation impacts the imaging performance.

The experimental geometry is chosen such that incorrect depth reconstruction will only affect the polar angle estimation in the Compton image. In this way, a detector with very poor depth reconstruction is expected to generate an elongated, oval shaped hot spot when imaging a point source [12]. A detector with good depth reconstruction should generate a circular hot spot. Thus, the image can be used to validate that the observed drift velocity nonuniformities degrade the depth resolution.

2. Experimental setup

All experimental procedures are conducted with two detectors (designated 4R10 and 4R61) that achieve energy resolution near 1% FWHM at 662 keV. These detectors are chosen to have similar spectral performance but significantly different imaging performance.

2.1. Gamma-ray measurement using a pixelated CdZnTe detector

When a detector is first received at the University of Michigan it is irradiated with ^{137}Cs gamma rays to evaluate crystal quality. Fifty million ^{137}Cs gamma-ray events are recorded in each crystal. Data are taken using the VAS_UM/TAT4 ASIC from Gamma-Medica Ideas [1]. The ^{137}Cs photopeak events are used to determine the amplitude and drift time distribution from each voxel of the detector. The results of this testing procedure are used to identify detectors with depth reconstruction problems.

2.2. Electron drift velocity measurement from alpha waveforms

In order to measure the drift time, a measurement system capable of reading out cathode waveforms is required, as the

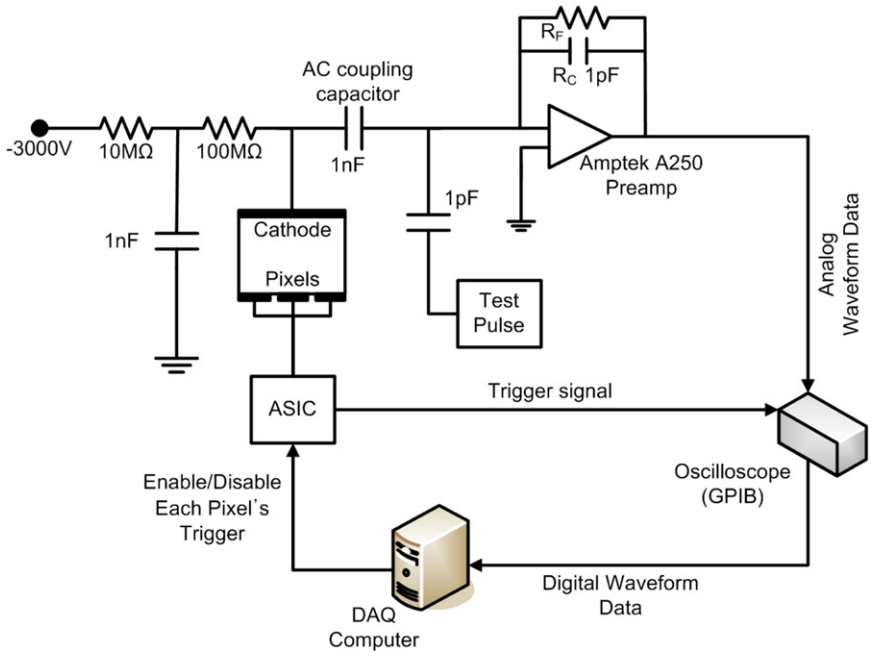

Fig. 2. Overview of the system used to measure waveforms generated from the cathode of pixelated CdZnTe detectors with an Amptek A250 preamplifier.

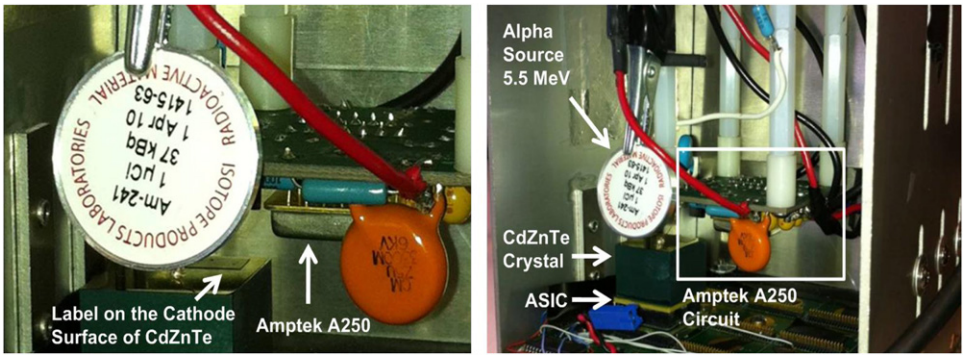

Fig. 3. System setup for measuring the electron drift velocity.

system described in Section 2.1 only provides information about amplitudes and drift times of the triggered pixels.

Fig. 2 is the overview of the system used to obtain cathode signals from CdZnTe detectors. An Amptek A250 preamplifier is added to the ASIC readout system in order to extract cathode waveforms from the detector while minimizing electronic noise. The output of the Amptek A250 is passed to an oscilloscope with an 8-bit ADC for digitization and readout. The oscilloscope readout only occurs when a trigger signal is received from the ASIC.

An ^{241}Am alpha source ($\sim$5.5 MeV) is used to generate cathode waveforms. Alpha particles are chosen because they deposit their substantial energy close to the surface of the device. When the source is placed above the cathode side it results in large electron signals, with excellent signal-to-noise ratios, that are known to be the result of electron drift through the entire thickness of the detector. Fig. 3 shows the system setup and the position of the alpha source. The distance from the alpha source to each pixel ranges from 15 mm to 25 mm resulting in alpha striking the cathode with energy between 3.8 MeV and 4.6 MeV.

An important goal of this work is to understand the spatial variance of drift time. However, the cathode waveform does not provide the position of each interaction. This information can be determined based on which pixel collects charge. The scope is triggered exclusively by the ASIC and the ASIC is configured such that only one pixel can trigger at any given time. In this way, the interaction position of each waveform is known based on which pixel is currently enabled. It is critical to increase the anode trigger threshold during this process to a much higher value than is used for gamma rays. This will prevent the pixels that neighbor the collecting pixel from generating an undesired trigger signal.

2.3. Compton imaging from a pixelated CdZnTe detector

A gamma-ray source is placed one meter from the detectors and positioned to irradiate one surface of each detector. It is important that the source not be located directly above the cathode or the anode or else the impact of the depth reconstruction on the image will be small. Data are collected for one hour and multiple interaction photopeak events are used to form an image for each detector. A the 511 keV emissions from a ^{22}Na source are used in this experiment. The 511 keV emission is preferred over the 662 keV emission from ^{137}Cs for this experiment because the average separation distance between interactions is smaller, which makes the image more sensitive to the reconstructed depth of each interaction.

3. Methods

3.1. Cathode waveforms measured from alpha source

The measurement configuration described in Section 2.2 is used to obtain cathode waveforms from the oscilloscope. Fig. 4 shows waveforms from one pixel with uniform drift velocity and another pixel with nonuniform drift velocity. The slope of the cathode waveform is a direct measure of the electron drift velocity at each depth. Because the energy of alpha particles is fully deposited at the cathode surface, the cathode signal reveals the electron drift velocity throughout the entire the detector thickness.

Several filters and correction methods should be applied to the cathode signals in order to effectively compare the waveforms from each pixel, as shown in Fig. 5. Filters are used to eliminate pile-up and gamma-ray events. If a cathode waveform approaches the upper limit of the range on the ADC then the event is characterized as pile-up and discarded. After excluding these events the baseline of all waveforms are aligned. To further reduce pile-up and eliminate gamma-ray events, only a limited range of pulse amplitudes are considered for analysis in each pixel. This range is determined based on the centroid of the alpha peak. Events that exceed the alpha-peak amplitude by more than 15% are classified as pile-up and discarded. Events that are less than 50% of the alpha-peak amplitude are classified as gamma-ray events and are also discarded. Using this wide range of amplitudes guarantees the alpha particles that experience significant electron trapping are still included in the analysis. The variation in attenuation through the air should have a small impact on the peak width, with less than a 3% incident energy fluctuation within the area of each pixel. Ultimately, these filters eliminate less than 5% of the total waveforms for each pixel.

Fig. 6(a) shows the cathode waveforms from two detectors after applying the pile-up filter, baseline correction, and amplitude filter collected. The waveforms have different amplitudes due to varying attenuation of alpha particles in the air, based on the path length from the source to each pixel. These variations can also be due to attenuation within the alpha source, varying inactive thickness on the surface of the CdZnTe, and energy straggling in the air attenuation process. Thus, the amplitude of each cathode waveform is normalized, as shown in Fig. 6(b), to allow for direct comparison of the drift profiles between any two events. It should be noted that the energy of the incident alpha particles will not affect the result of this experiment as long as it is large enough to result in a adequate signal-to-noise ratio. The key information for this experiment is in the profile of the charge induction over time, not the absolute magnitude.

Another important factor is that the ASIC trigger is generated from the pixels, which represents the collection time, or the end of the alpha pulse. It is much easier to compare the shape of the alpha waveforms if they are aligned at the beginning of the charge induction. In order to align the initial rise, a time shift is applied to each cathode waveform, with the result shown in Fig. 6(c).

3.2. Drift time measurement from gamma-ray data

The ^{137}Cs gamma-ray data are analyzed on a pixel-by-pixel basis. All of the single pixel photopeak events are assigned a depth bin based on their C/A ratio. The drift time of each event is measured in order to form a timing spectrum for each depth bin of each pixel. Fig. 7 shows the timing spectra for each depth of one pixel in detector 4R61. The average drift time and the drift time uncertainty for each depth is measured from the timing spectrum. The relationship between the raw timing output from the ASIC and the drift time is calibrated by measuring the ASIC timing signal associated with a known delay.

3.3. Drift time from each depth estimated by cathode waveforms

The VAS_UM/TAT4 ASIC used in this experiment can measure the drift time associated with each depth. The same information can be derived from the alpha waveforms to validate the drift time values determined from the ASIC data. It is assumed that the signal amplitude can be directly converted to the depth of the electron cloud, as the weighting potential for the cathode is linear [13], each

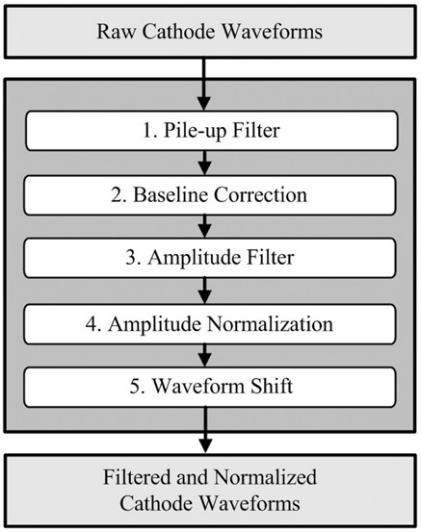

Fig. 5. Summary of the filters and correction methods that are applied to the raw cathode waveforms.

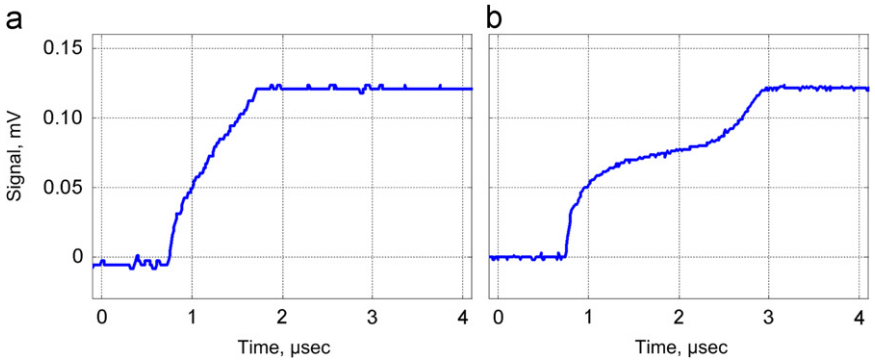

Fig. 4. The cathode signals from an Amptek A250 preamp triggered by an ASIC anode pixel with either uniform (left) or nonuniform (right) electron drift velocity. For convenience, the value of cathode signals is multiplied by −1. (a) Uniform electron drift velocity and (b) Non-uniform electron drift velocity.

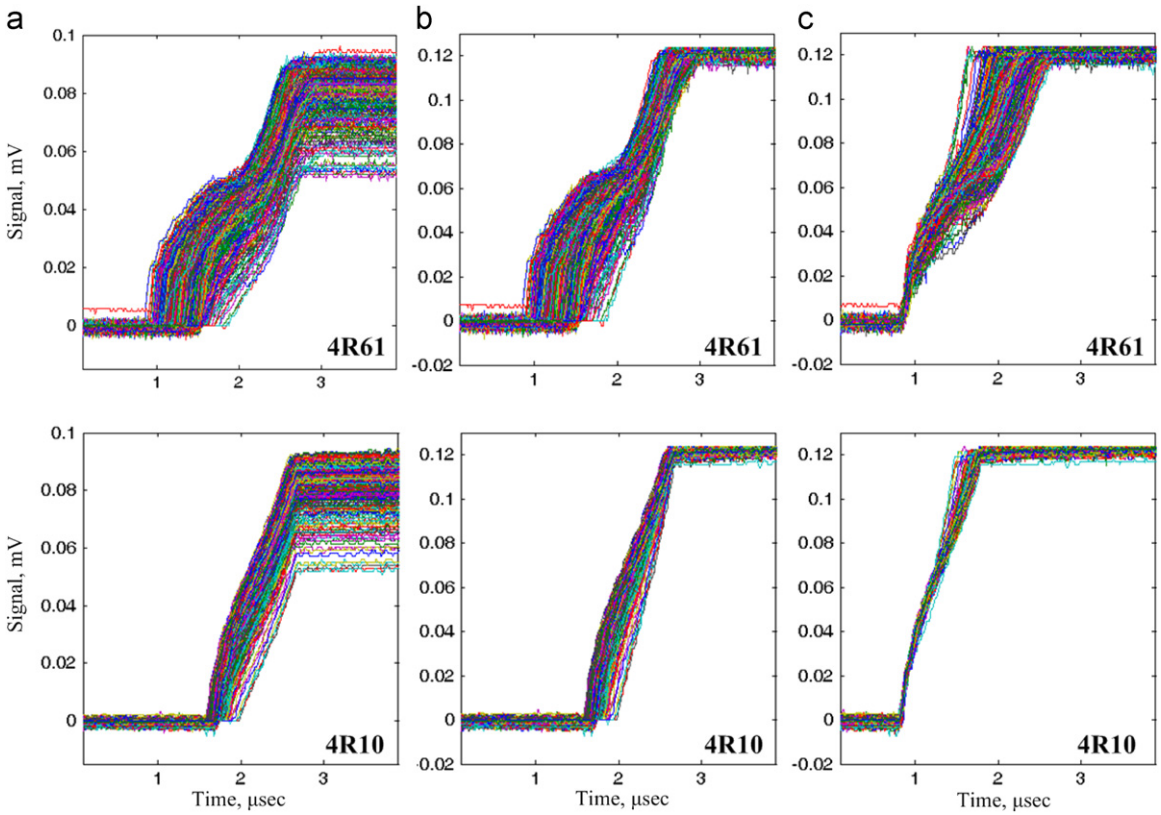

Fig. 6. The cathode signal waveforms in (a) are the result of applying only the pile-up filter, baseline correction, and the amplitude filter. The cathode signal waveforms in (b) include normalization (norm.) and the waveforms in (c) also include waveform shift (shift) correction. The cathode signals are obtained for pixel (5,7) in 4R61 and pixel (10,2) in 4R10. (a) No norm. and shift, (b) After norm. only and (c) After norm. and shift.

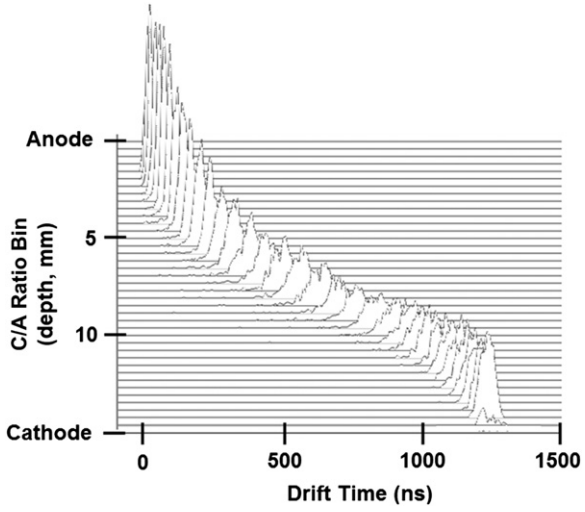

Fig. 7. The drift time distribution for each depth in one pixel of detector 4R61. Drift time values are shown for photopeak events from a measurement with a ^{137}Cs gamma-ray source.

waveform is due to a surface interaction of an alpha particle, and electron trapping is consistently less than 5% in this detector. Fig. 8 shows the technique for measuring the drift time for a particular depth of interaction based on alpha waveforms. The drift time is measured for each sample of the alpha waveform as the time difference between the sample point and the point when the waveform reaches its maximum amplitude. The drift time for each depth bin, as defined in the gamma-ray measurement, is calculated for every alpha waveform in order to generate an average drift time and a drift time distribution from alpha data.

3.4. Compton imaging from gamma-ray measurement

The Compton image is formed using standard back-projection techniques [12]. Only photopeak events that occur in two separate pixels are used. If the two pixels are side-by-side neighbors the events are not used for imaging purposes. The cone angle uncertainty is calculated for each event based on the system model. More than 20,000 total events are used to form each image in order to get an accurate indication of the image quality of each detector.

4. Results and analysis

4.1. Cathode waveforms from alpha particles

Fig. 9 shows the number of counts measured for each anode pixel position after 5 min of measurement per pixel. There are some locations with very few waveforms due to a label applied to the cathode surface of the detector as well as a high voltage wire that is attached to the cathode with epoxy. These pixels will be discarded from future analysis in this paper. The alpha source is not centered directly above the cathode, resulting in a variable separation distance between the source and each pixel, such that the number of counts and alpha peak centroid decreases gradually from the right to left side of the detector, evident from the count data in Fig. 9.

Fig. 10 shows cathode waveforms in each pixel after applying the pile-up filter, baseline correction, amplitude filter, normalization, and waveform shift. The measured alpha data clearly show that the electron drift velocities vary along the drift trajectory. The electron drift velocity in the middle of detector

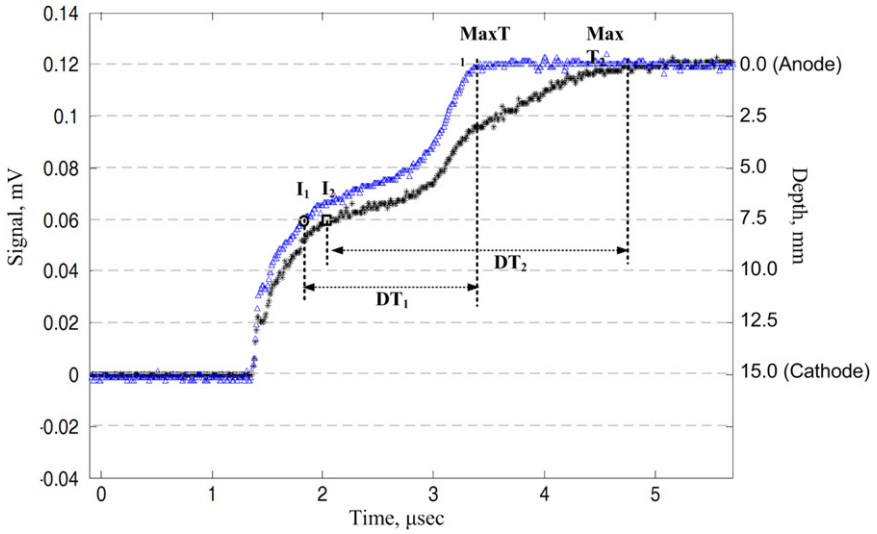

Fig. 8. Drift time measurement from each depth using alpha waveform data. Two different waveforms are shown from the same pixel of detector 4R61. The depth at each time is determined from the signal amplitude. The figure shows the calculation of the drift time (DT_1 and DT_2) associated with an interaction that occurs near the center depth of the detector.

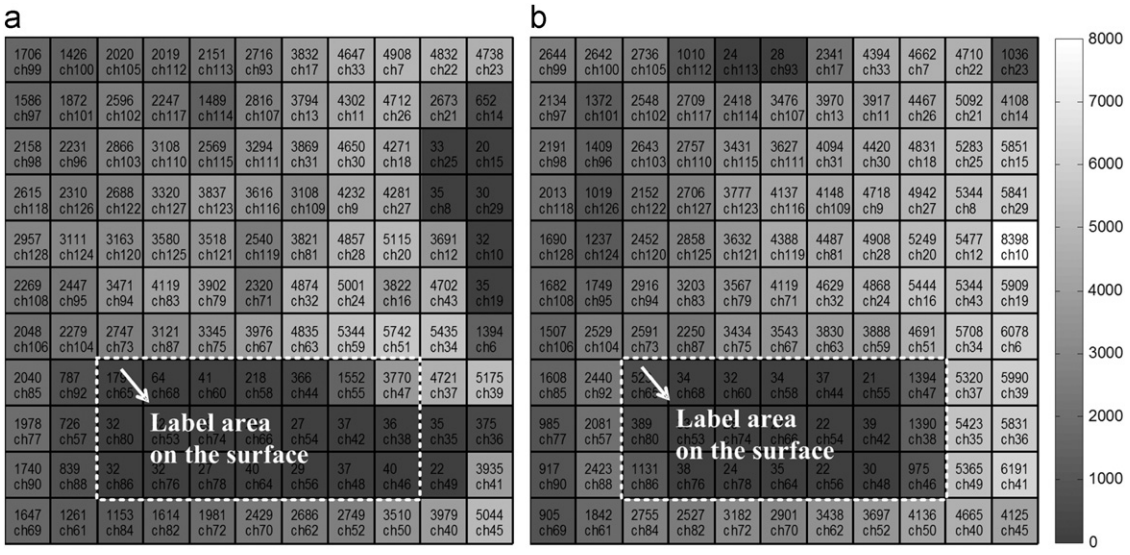

Fig. 9. The number of raw cathode waveforms in each of the 11×11 anode pixels after 5 min of alpha source counting. (a) 4R61 and (b) 4R10.

4R61 is slower than near the cathode and anode. This means that either the electric field or the electron mobility near the cathode and anode must be greater than in the middle of the crystal. This effect has been observed in many of the Redlen detectors tested at the University of Michigan.

The data for detector 4R61 show that the electron drift profiles from a single pixel can have significant variation. In the case of gamma rays this will result in variable drift times within each voxel. Accurate depth reconstruction will be impossible using the readout scheme such as the VAS_UM/TAT4 ASIC with spatial resolution limited by the pixel pitch. Currently, the depth correction for multiple-pixel events uses the averaged electron drift time in each pixel. Thus, pixelated CdZnTe detectors with significant nonuniformity of electron drift velocities cannot avoid poor depth correction for multiple-pixel events.

4.2. Drift time measurement based on gamma rays

Figs. 11 and 12 show the average and the uncertainty of the drift time as a function of depth for each pixel measured with ^{137}Cs (662 keV) gamma rays. The drift time uncertainty is reported as the standard deviation. There are many regions of detector 4R61 that show long drift times relative to detector 4R10. Furthermore, in these regions of very slow electron drift the standard deviation of the drift time increases significantly, by a factor of five or more.

A systematic increase in the drift time uncertainty of detector 4R61 is well correlated to the pixels that demonstrated nonuniform drift velocities when irradiated with alphas. This provides evidence that the gamma-ray data is a useful indicator of drift velocity variation. However, there are limitations when the gamma-ray data is used to measure drift time variation. The uncertainty in the drift time will be influenced by the jitter associated with the ASIC timing measurement. This jitter is most extreme in the regions where the cathode signal rises slowly. Thus, the regions in the center of the detector, with the lowest electron drift velocity, consistently result in the greatest drift time uncertainty.

There is a limit on the maximum measured drift time due to the fixed time interval between the system trigger and system

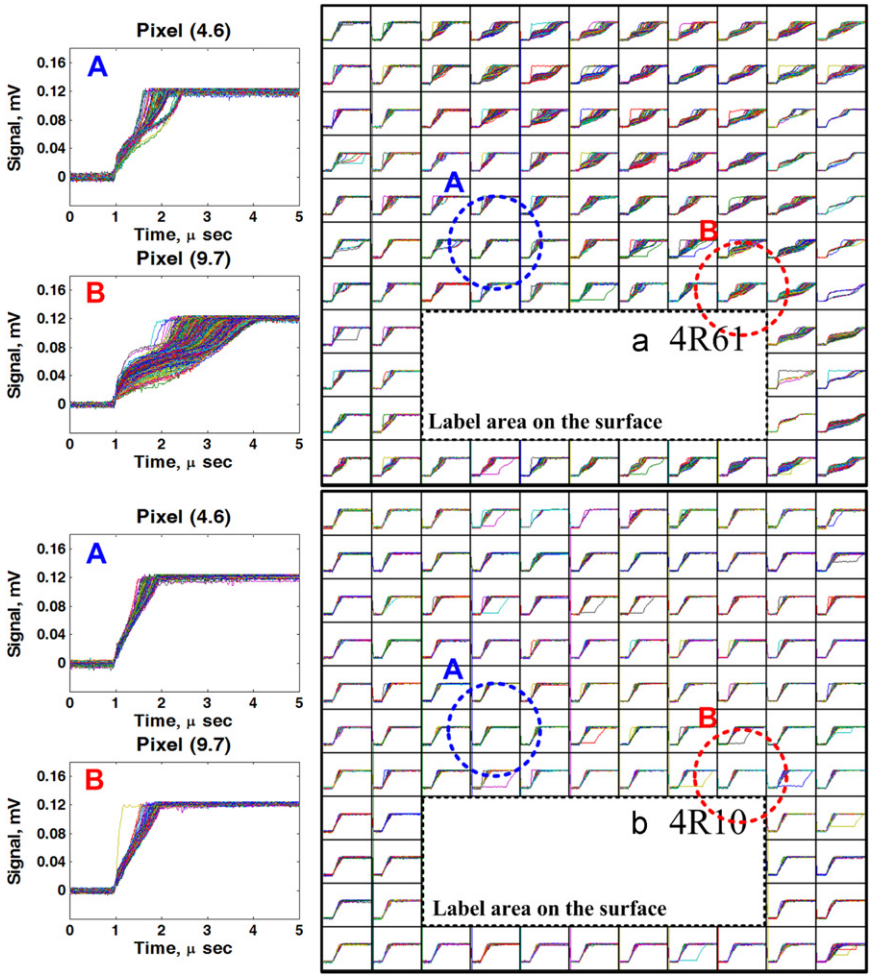

Fig. 10. The final cathode waveforms in each pixel of two CdZnTe crystals (4R61 and 4R10) when all waveform corrections are applied. All the waveforms that passed the pile-up and amplitude filters are shown for each pixel. The horizontal axis is the time (μs), from cathode to anode. The vertical axis is the signal (mV).

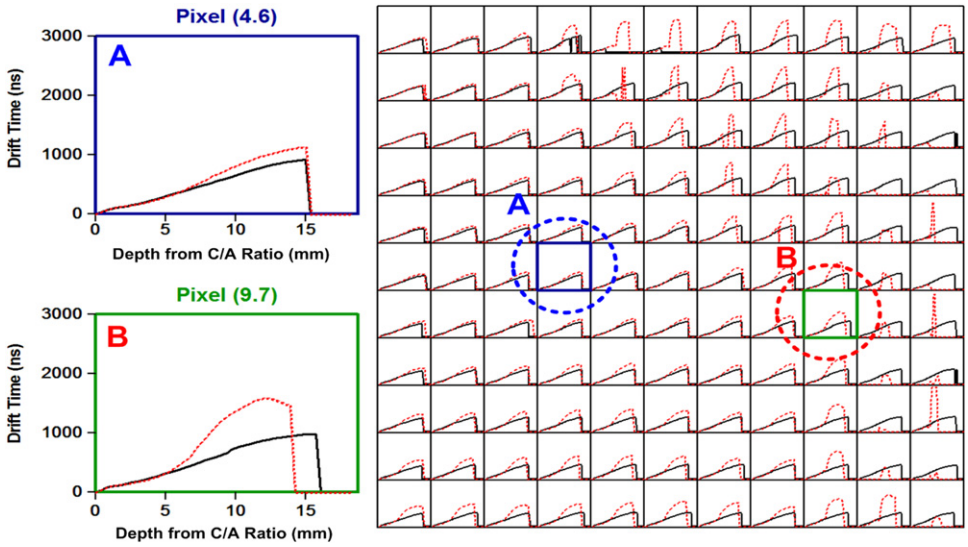

Fig. 11. Average drift time for each pixel measured with ^{137}Cs (662 keV) using two CdZnTe detectors: 4R10 (solid lines) and 4R61 (dotted lines). The horizontal axis represents the depth of interaction within the crystal, from anode (0 mm) to cathode (15 mm).

readout. This results in a loss of data near the cathode side for pixels with a drift time longer than 2.5 μs. In the drift time uncertainty data there is an increase in the timing uncertainty near the anode. This is because the C/A ratio is no longer linear near the anode surface and a single C/A ratio bin represents a large range of timing values.

In order to eliminate the possibility of the steering electrode affecting the drift velocity profile within a single pixel, these

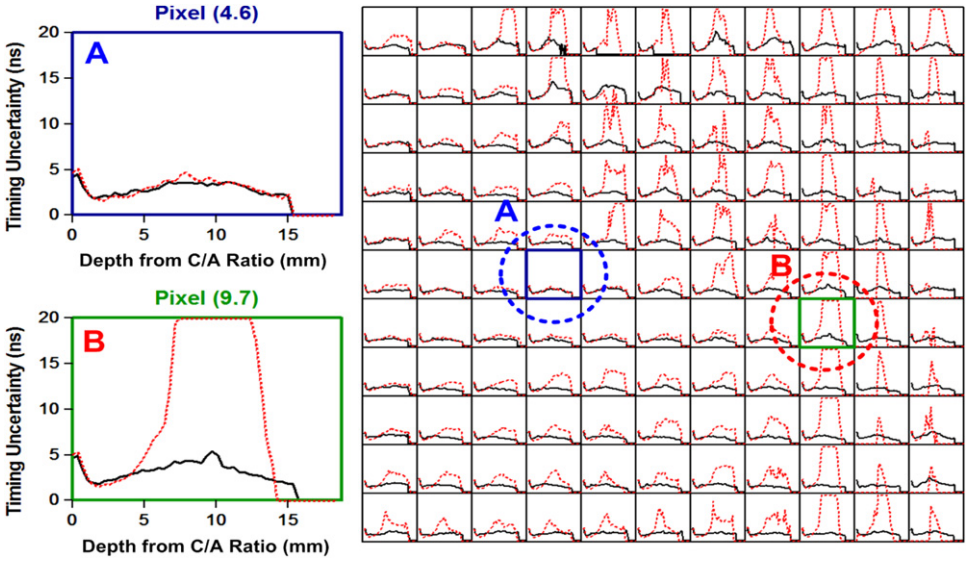

Fig. 12. Drift time uncertainty for each pixel measured with ^{137}Cs (662 keV) using two CdZnTe detectors: 4R10 (solid lines) and 4R61 (dotted lines). The horizontal axis represents the depth of interaction within the crystal, from anode (0 mm) to cathode (15 mm).

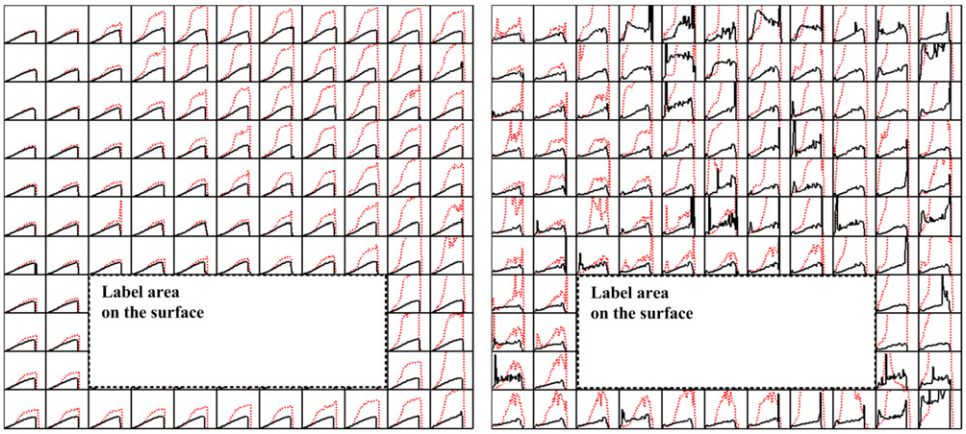

Fig. 13. Average drift time (left) and drift time uncertainty (right) for each pixel measured from cathode waveforms generated by alpha particles incident on detector 4R10 (solid lines) and 4R61 (dotted lines). The horizontal and vertical scale for each pixel are identical to the axes shown in Figs. 11 and 12.

experiments have been also repeated without bias on the steering electrode. The same patterns described in the above analysis are duplicated when the steering bias is set to zero.

4.3. Drift time measurement based on alpha particles

Fig. 13 shows the average and the uncertainty of the drift time calculated from alpha waveforms. The trends in the alpha data are closely matched with those observed in the gamma-ray data; the pixels in the upper right corner of detector 4R61 have long drift times from cathode to anode and large drift time uncertainty in the central depths while all pixels in detector 4R10 show a uniform response at all depths.

The alpha data provides a more complete picture than the gamma-ray data. Unlike the gamma-ray data, the alpha data can provide drift time data very close to the anode and the cathode. There is no upper limit on the maximum drift time measured, assuming the entire waveform can be captured by the scope. As a result, the cathode waveform analysis can measure drift times much longer than 3 μs. Furthermore, the time jitter associated with the alpha-particle drift time measurement is much smaller than for the gamma-ray measurement. Therefore, the alpha-particle data shows the true fluctuation in the total drift time at each depth, which increases systematically from anode to cathode.

4.4. Gamma-ray imaging performance

Fig. 14 is the reconstructed image from CdZnTe detectors (4R10 and 4R61) using ^{22}Na (511 keV) source. As expected, detector 4R61 produces a much poorer image than detector 4R10. Furthermore, the image distortion is consistent with the expectation for a detector with poor depth reconstruction, as predicted mathematically in Ref. [12]. Specifically, the uncertainty in the azimuthal dimension is fairly similar between the two detectors, at 45° for detector 4R10 and 54° for detector 4R61. The polar dimension, however, shows a sharp disagreement between the two detectors, with a FWHM of 56° for detector 4R10 and 82° for detector 4R61. This significant degradation in the image quality illustrates the importance of the depth reconstruction on the overall device performance.

5. Summary

This work has provided experimental evidence of nonuniform drift velocity within a pixel, nonuniform drift time within a voxel, and

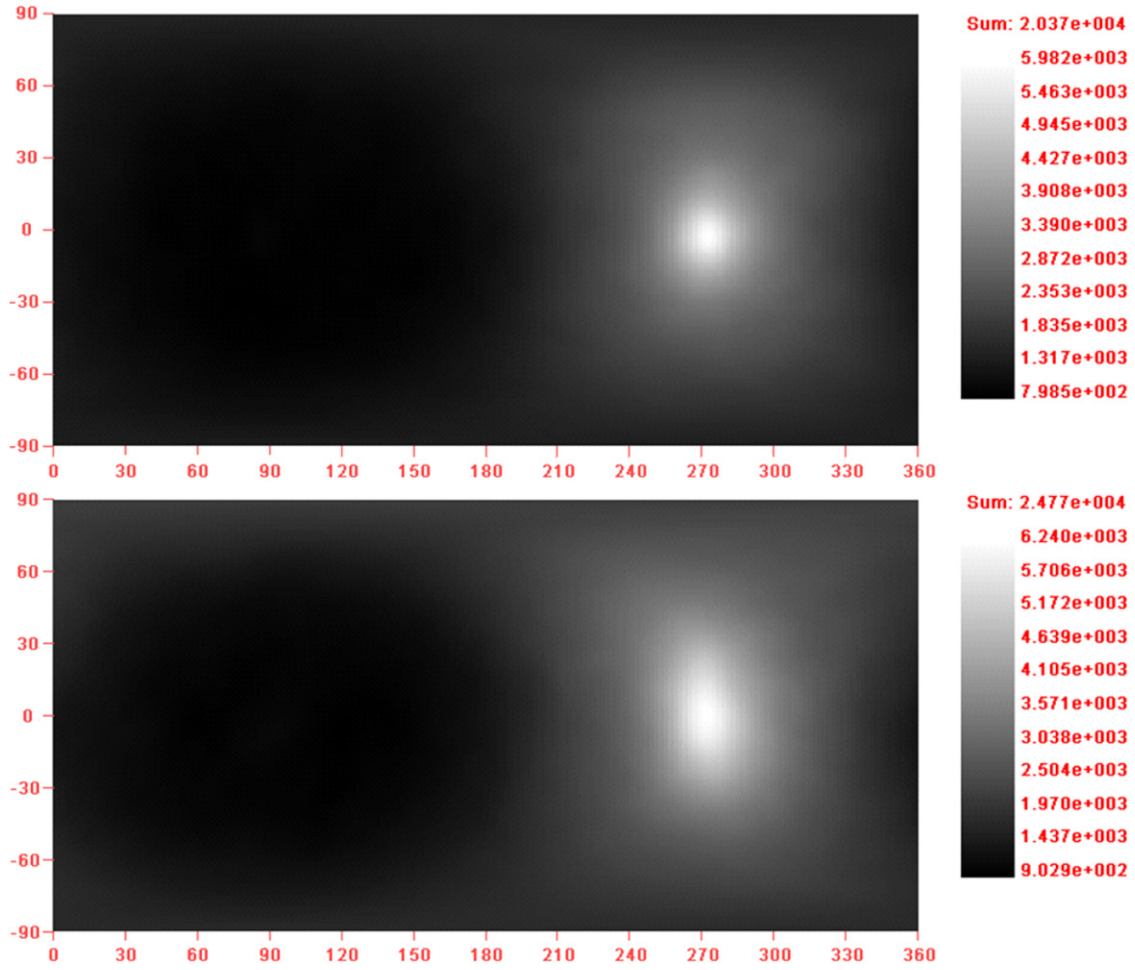

Fig. 14. The reconstructed image from the two CdZnTe detectors 4R10 (top) and 4R61 (bottom) using a ^{22}Na source. Simple back projection is used to generate an image from the 511 keV photopeak events.

the impact of these nonuniformities on the reconstructed depth of interaction. Results from two different techniques used to measure the nonuniformity of drift time and drift velocity are presented: one technique is based on gamma-ray interactions at different depths and the other is based on the drift of electrons through the detector due to alpha interactions on the cathode surface. An ASIC is used to readout the gamma-ray data while a digital pulse processing is applied to the alpha waveforms. Ultimately, the results are very similar for the two detectors tested. One detector, 4R10, is found to be quite uniform while the other detector, 4R61, has regions of very slow electron drift. The drift time within each voxel is shown to vary significantly in the regions of low electron drift velocity.

In pixelated CZT detectors, multiple-pixel events caused by multiple interaction gamma-ray events permit Compton imaging. However, these multiple-pixel events also require accurate drift time measurement for correct depth reconstruction. The impact of the drift time variation is demonstrated by forming a Compton image with each detector. The angular resolution in the polar dimension degrades by almost 50% in detector 4R61 relative to detector 4R10.

This work shows that the gamma-ray measurement performed with the VAS_UM/TAT4 ASIC is a good indicator of electron transport problems that will degrade the overall system performance.

Acknowledgments

This work is supported by DOE NA-22 office (award number DE-FG52-06NA27499).

References

[1] F. Zhang, Z. He, IEEE Transactions on Nuclear Science NS-53 (October (5)) (2006) 3021, http://dx.doi.org/10.1109/TNS.2006.879761. ISSN: 0018-9499.
[2] F. Zhang, Z. He, C.E. Seifert, IEEE Transactions on Nuclear Science NS-54 (August (4)) (2007) 843, http://dx.doi.org/10.1109/TNS.2007.902354. ISSN: 0018-9499.
[3] Z. He, W. Li, G.F. Knoll, D.K. Wehe, J. Berry, C.M. Stahle, Nuclear Instruments and Methods in Physics Research Section A: Accelerators, Spectrometers, Detectors and Associated Equipment 422 (1–3) (1999) 173, http://dx.doi.org/10.1016/S0168-9002(98)00950-4. ISSN: 0168-9002, URL 〈http://www.sciencedirect.com/science/article/pii/S0168900298009504〉.
[4] A.E. Bolotnikov, S.O. Babalola, G.S. Camarda, H. Chen, S. Awadalla, Y. Cui, S.U. Egarievwe, P.M. Fochuk, R. Hawrami, A. Hossain, J.R. James, I.J. Nakonechnyj, J. Mackenzie, G. Yang, C. Xu, R.B. James, IEEE Transactions on Nuclear Science NS-56 (4) (2009) 1775, http://dx.doi.org/10.1109/TNS.2009.2019960. ISSN: 0018-9499.
[5] A.E. Bolotnikov, S. Babalola, G.S. Camarda, Y. Cui, R. Gul, S.U. Egarievwe, P.M. Fochuk, M. Fuerstnau, J. Horace, A. Hossain, F. Jones, K.H. Kim, O.V. Kopach, B. McCall, L. Marchini, B. Raghothamachar, R. Taggart, G. Yang, L. Xu, R.B. James, IEEE Transactions on Nuclear Science NS-58 (August (4)) (2011) 1972, http://dx.doi.org/10.1109/TNS.2011.2160283. ISSN: 0018-9499.
[6] A. Burger, M. Groza, Y. Cui, D. Hillman, E. Brewer, A. Bilikiss, G. Wright, L. Li, F. Lu, R. James, Journal of Electronic Materials 32 (2003) 756, http://dx.doi.org/10.1007/s11664-003-0066-6. ISSN: 0361-5235.
[7] A.E. Bolotnikov, G.S. Camarda, Y. Cui, A. Hossain, G. Yang, H.W. Yao, R.B. James, IEEE Transactions on Nuclear Science NS-56 (June (3)) (2009) 791, http://dx.doi.org/10.1109/TNS.2008.2007904. ISSN: 0018-9499.
[8] A.E. Bolotnikov, J. Butcher, G.S. Camarda, Y. Cui, S.U. Egarievwe, P. Fochuk, R. Gul, M. Hamade, A. Hossain, K. Kim, O.V. Kopach, M. Petryk, B. Raghothamachar, G. Yang, R.B. James, SPIE 8142 (2011) 814206, http://dx.doi.org/10.1117/12.896223. URL 〈http://link.aip.org/link/?PSI/8142/814206/1〉.
[9] J.C. Kim, S.E. Anderson, W. Kaye, F. Zhang, Y. Zhu, S.J. Kaye, Z. He, Nuclear Instruments and Methods in Physics Research Section A: Accelerators, Spectrometers, Detectors and Associated Equipment 654 (1) (2011) 233, http://dx.doi.

org/10.1016/j.nima.2011.06.038. ISSN: 0168-9002, URL 〈http://www.sciencedirect.com/science/article/pii/S0168900211011545〉.

[10] Z. He, G.F. Knoll, D.K. Wehe, J. Miyamoto, Nuclear Instruments and Methods in Physics Research Section A: Accelerators, Spectrometers, Detectors and Associated Equipment 388 (1–2) (1997) 180, http://dx.doi.org/10.1016/S0168-9002(97)00318-5. ISSN: 0168-9002, URL 〈http://www.sciencedirect.com/science/article/B6TJM-3SPKDP1-1W/2/afa1bd845c5c6e90aa9bbc141c58c3fd〉.

[11] Y. Zhu, S.E. Anderson, Z. He, IEEE Transactions on Nuclear Science NS-58 (June (3)) (2011) 1400, http://dx.doi.org/10.1109/TNS.2011.2132738. ISSN: 0018-9499.

[12] W. Wang, Compton Imaging Techniques for Position-Sensitive Gamma-ray Detectors and How They Can Be Useful, PhD Thesis, University of Michigan, 2011.

[13] Z. He, Nuclear Instruments and Methods in Physics Research Section A: Accelerators, Spectrometers, Detectors and Associated Equipment 463 (2001) 250.